

# Giant vortex in a harmonically-trapped rotating dipolar $^{164}\text{Dy}$ condensate

Luis E. Young-S.<sup>a</sup>, S. K. Adhikari<sup>b</sup>

<sup>a</sup>*Grupo de Modelado Computacional y Programa de Matemáticas, Facultad de Ciencias Exactas y Naturales, Universidad de Cartagena, 130015 Cartagena de Indias, Bolívar, Colombia*

<sup>b</sup>*Instituto de Física Teórica, UNESP - Universidade Estadual Paulista, 01.140-070 São Paulo, São Paulo, Brazil*

---

## Abstract

We demonstrate the formation of dynamically stable giant vortices in a harmonically-trapped strongly dipolar  $^{164}\text{Dy}$  Bose-Einstein condensate under rotation around the polarization direction of dipolar atoms, employing the numerical solution of an improved mean-field model including a Lee-Huang-Yang-type interaction, meant to stop a collapse at high atom density. These giant vortices are stationary, obtainable by imaginary-time propagation using a Gaussian initial state, while the appropriate phase of the giant vortex is imprinted on the initial wave function. The dynamical stability of the giant vortices is established by real-time propagation during a long interval of time after a small change of a parameter.

---

## 1. Introduction

After the observation of harmonically-trapped Bose-Einstein condensates (BEC) of alkali-metal atoms at ultra-low temperatures in a laboratory [1, 2], there have been many experiments to investigate their superfluid properties. An earmark of superfluidity is the generation of a quantized vortex in a rotating BEC. According to Onsager [3], Feynman [4], and Abrikosov [5] these vortices have quantized circulation [6]:

$$\frac{m}{2\pi\hbar} \oint_C \mathbf{v} \cdot d\mathbf{r} = \pm l, \quad (1)$$

where  $\mathbf{v}(\mathbf{r}, t)$  is superfluid velocity at point  $\mathbf{r}$  and time  $t$ ,  $l$  is the quantized angular momentum of an atom in unit of  $\hbar$ ,  $m$  is its mass,  $C$  is a generic closed path. For  $l \neq 0$ , a quantized vortex line appears [6] due to topological defects inside the closed path  $C$ .

Under slow and rapid rotational velocity, a quantized vortex [7, 8, 9, 6] and a vortex-lattice structure [10] were created, respectively, in a rotating BEC under controlled conditions and were experimentally investigated. With the increase of the angular velocity of rotation of a harmonically-trapped BEC, many vortices of unit angular momentum each per atom ( $l = 1$ ) are formed on an Abrikosov triangular lattice [5]. An angular momentum state with  $l > 1$  in a single-component

harmonically-trapped BEC [7, 10, 11, 12, 13] is unstable from an energetic consideration and decays into multiple vortices of unit angular momentum each. In a multicomponent spinor BEC one can also have the formation of square [14, 15, 16, 17], stripe and honeycomb [18] vortex lattice, different from the triangular Abrikosov lattice [5]. Moreover, it is possible to create coreless vortices [19], fractional angular momentum vortices [20, 21] and phase-separated vortex lattices in multi-component spinor [22] and dipolar [15, 16] BECs.

In spite of continued efforts [23], it has not been possible to generate a giant vortex of large angular momentum ( $l > 1$ ) in a harmonically trapped BEC. In addition to theoretical interest, such a vortex could be useful in quantum information processing [24, 25]. The existence of a giant vortex in a BEC confined by a quadratic plus a quartic trap, [26, 27, 28, 29, 30, 31, 32], a bubble trap [33] or a Gaussian plus a quadratic trap [34] have also been theoretically predicted. In all these cases the effective trapping potential develops a repulsion in the central region, like a Mexican hat potential, resulting in a hole along the rotation axis which accommodates a giant vortex. It was also possible to observe a dynamically-formed metastable giant vortex of large angular momentum ( $60 > l > 7$ ) in a rapidly-rotating harmonic trap [35] and investigate it numerically [36]. There has been significant work on the creation of giant vortices in a regular BEC as a negative temperature state [37]. A giant vortex in a multicomponent nondipolar [38, 39, 40] and dipolar [41] BEC and also in a spin-

---

*Email addresses:* lyoung@unicartagena.edu.co (Luis E. Young-S.), sk.adhikari@unesp.br (S. K. Adhikari)

orbit coupled BEC [40] was also studied.

In view of the above, it is highly desirable to have a giant vortex in a single-component harmonically-trapped BEC, if that is at all possible. To this end we demonstrate the formation of giant vortices of large angular momentum ( $5 \geq l \geq 2$ ) in a harmonically-trapped BEC of  $^{164}\text{Dy}$  atoms, with large dipole moment, under rotation around the polarization direction  $z$  of the dipolar atoms. Previously, significant work was done on dipolar systems with rotation [42, 43], although no giant vortex was reported. To avoid a collapse of the strongly dipolar atoms, we used an improved mean-field model, where we include a Lee-Huang-Yang-type (LHY) interaction [44], appropriate for dipolar atoms [45, 46, 47]. As the dipolar interaction increases beyond a critical value [48, 49], a strongly dipolar BEC collapses in the mean-field Gross-Pitaevskii (GP) model. However, if a LHY interaction [45, 47] is included in the same model, the collapse can be avoided and the dipolar BEC can be stabilized [50]. The same model including the LHY interaction was used recently in the study of the formation of droplets in a strongly dipolar BEC of dysprosium and erbium atoms [50] as well as the formation of lattice [51, 52] and other structures [53, 54] in that system. In this study, the number of atoms is taken as  $N = 200000$  and the scattering length  $a$  is taken to be  $a = 80a_0$ , close to the previously employed estimates  $92(8)a_0$  [55],  $87(8)a_0$  [56] and  $a = 88a_0$  [51], where  $a_0$  is the Bohr radius. The angular frequency  $\omega_z$  of the confining trap in the direction of polarization  $z$  of the dipolar atoms is taken to be  $\omega_z = 2\pi \times 167$  Hz, as in some experimental [57, 58] and theoretical [51, 52] studies on a dipolar BEC of  $^{164}\text{Dy}$  atoms, whereas the angular frequencies of the confining circularly-symmetric trap in the transverse  $x$  and  $y$  directions are taken to be  $\omega_x = \omega_y \equiv \omega_\rho = 0.75\omega_z$ . The number of atoms, scattering length and the trap parameters for the formation of a giant vortex in the strongly-dipolar BEC of  $^{164}\text{Dy}$  atoms are quite similar to those used in recent experiments [50, 57, 58]. The angular velocity of rotation is taken in the range  $0 < \Omega < 0.5\omega_z$  which, for  $\omega_\rho = 0.75\omega_z$ , is equivalent to  $\Omega < 2\omega_\rho/3$ , which is not very high as it can go as high as  $\Omega \rightarrow \omega_\rho$  [6] for an ordered rotation of the BEC. For this set of parameters the ground state of a strongly-dipolar nonrotating  $^{164}\text{Dy}$  BEC naturally develops a hole along the  $z$  axis [59] as in a Mexican-hat potential [26, 27, 34] to have a hollow cylindrical shape and when set into rotation this BEC can accommodate a stationary giant vortex of angular momentum up to  $l = 5$ .

It is pertinent to ask what is so different in the strongly dipolar  $^{164}\text{Dy}$  BEC, from a nondipolar BEC, considered

so far in search of a giant vortex, that will stabilize a giant vortex. The combined action of the long-range non-local dipolar interaction and the collapse inhibiting LHY interaction in the improved mean-field model allows the formation of giant vortices in a harmonically-trapped strongly dipolar BEC. The in-plane dipolar repulsion in the  $x$ - $y$  plane and the centrifugal repulsion in the rotating condensate create a hollow region along the  $z$  direction in a giant vortex, which is stabilized by the harmonic trap and the strongly repulsive LHY interaction. The harmonic trap stops the outward expansion of the giant vortex and the strongly repulsive LHY interaction stops its inward collapse, thus stabilizing the giant vortex. Although a multiple-charge vortex is unstable in the presence of matter, it can be stabilized in this central hollow region as found also in a BEC with an effective Mexican hat type potential [26, 27, 34] responsible to create a central hollow region.

In Sec. 2 a description of the the mean-field model, with the appropriately modified [45, 47] LHY interaction [44], for a rotating dipolar BEC, with repulsive atomic interaction (positive scattering length), is presented. A variational estimate of the energy of the rotating dipolar BEC is also given. In Sec. 3 we display numerical results for the formation of stationary giant vortices in strongly dipolar BECs as obtained by imaginary-time propagation. For the chosen set of parameters we could stabilize a giant vortex of angular momentum  $l \leq 5$ . The numerical energy of the giant vortices follows a simple theoretical formula [6]. The dynamical stability of the giant vortices was established by a steady real-time propagation over a long interval of time of a giant-vortex, after introducing a small perturbation, using the converged imaginary-time wave function as the initial state. In Sec. 4 we present a brief summary of our findings.

## 2. Improved mean-field model

The improved GP equation for a dipolar BEC of  $N$  atoms, of mass  $m$  each, after the inclusion of the LHY interaction, appropriate for dipolar atoms, can be written as [60, 61, 62, 63]

$$i\hbar \frac{\partial \psi(\mathbf{r}, t)}{\partial t} = \left[ -\frac{\hbar^2}{2m} \nabla^2 + V(\mathbf{r}) + \frac{4\pi\hbar^2}{m} aN |\psi(\mathbf{r}, t)|^2 + \frac{3\hbar^2}{m} a_{\text{dd}} N \int U_{\text{dd}}(\mathbf{R}) |\psi(\mathbf{r}', t)|^2 d\mathbf{r}' + \frac{\gamma_{\text{LHY}} \hbar^2}{m} N^{3/2} |\psi(\mathbf{r}, t)|^3 \right] \psi(\mathbf{r}, t), \quad (2)$$

$$U_{\text{dd}}(\mathbf{R}) = \frac{1 - 3 \cos^2 \theta}{|\mathbf{R}|^3}, \quad a_{\text{dd}} = \frac{\mu_0 \mu^2 m}{12\pi \hbar^2}, \quad (3)$$

where  $V(\mathbf{r}) = \frac{1}{2}m[\omega_\rho^2(x^2 + y^2) + \omega_z^2z^2]$  is an axially-symmetric trap,  $\mu$  is the magnetic dipole moment of an atom,  $\mu_0$  is the permeability of vacuum,  $U_{\text{dd}}(\mathbf{R})$  is the anisotropic dipolar interaction between two atoms placed at  $\mathbf{r} \equiv \{\mathbf{x}, \mathbf{y}, \mathbf{z}\}$  and  $\mathbf{r}' \equiv \{\mathbf{x}', \mathbf{y}', \mathbf{z}'\}$  and  $\theta$  is the angle between the vector  $\mathbf{R} \equiv \mathbf{r} - \mathbf{r}'$  and the  $z$  axis,  $a_{\text{dd}}$  is the dipolar length which measures the strength of atomic dipolar interaction; the wave function normalization is  $\int |\psi(\mathbf{r}, t)|^2 d\mathbf{r} = 1$ .

The coefficient of the LHY interaction [44]  $\gamma_{\text{LHY}}$  in Eq. (2), as modified for dipolar atoms [45, 47], is given by [45, 46, 47]  $\gamma_{\text{LHY}} = \frac{128}{3} \sqrt{\pi a^5} Q_5(\varepsilon_{\text{dd}})$ ,  $\varepsilon_{\text{dd}} = \frac{a_{\text{dd}}}{a}$ , where  $Q_5(\varepsilon_{\text{dd}}) = \int_0^1 dx (1 - \varepsilon_{\text{dd}} + 3x^2\varepsilon_{\text{dd}})^{5/2}$  is the auxiliary function. For nondipolar atoms  $\varepsilon_{\text{dd}} = 0$ , while  $Q_5(\varepsilon_{\text{dd}}) = 1$ , and we get back the usual LHY coefficient [44]. The auxiliary function can be approximated as [61]

$$Q_5(\varepsilon_{\text{dd}}) = \frac{(3\varepsilon_{\text{dd}})^{5/2}}{48} \Re \left[ (8 + 26\eta + 33\eta^2) \sqrt{1 + \eta} + 15\eta^3 \ln \left( \frac{1 + \sqrt{1 + \eta}}{\sqrt{\eta}} \right) \right], \quad \eta = \frac{1 - \varepsilon_{\text{dd}}}{3\varepsilon_{\text{dd}}}, \quad (4)$$

subject to the limiting value  $Q_5(1) = 3\sqrt{3}/2$ , where  $\Re$  is the real part. In this paper we will use the analytic approximation (4) for  $Q_5(\varepsilon_{\text{dd}})$ .

The Hamiltonian of the rotating dipolar BEC in the rotating frame is given by [64]  $H = H_0 - \Omega l_z$ , where  $H_0$  is the Hamiltonian in the inertial frame and  $l_z \equiv i\hbar(y\partial/\partial x - x\partial/\partial y)$  is the  $z$  component of angular momentum and  $\Omega$  the angular velocity of rotation. Using this transformation, the mean-field GP equation (2) for the trapped BEC in the rotating frame for  $\Omega < \omega_\rho$  can be written as

$$i\hbar \frac{\partial \psi(\mathbf{r}, t)}{\partial t} = \left[ -\frac{\hbar^2}{2m} \nabla^2 + V(\mathbf{r}) + \frac{4\pi\hbar^2}{m} aN |\psi(\mathbf{r}, t)|^2 + \frac{3\hbar^2}{m} a_{\text{dd}} N \int U_{\text{dd}}(\mathbf{R}) |\psi(\mathbf{r}', t)|^2 d\mathbf{r}' + \frac{\gamma_{\text{LHY}} \hbar^2}{m} N^{3/2} |\psi(\mathbf{r}, t)|^3 - \Omega l_z \right] \psi(\mathbf{r}, t). \quad (5)$$

For  $\Omega > \omega_\rho$  a harmonically-trapped rotating BEC makes a quantum phase transition to a non-superfluid state, where a mean-field description of the rotating BEC might not be valid [6].

To write Eq. (5) in the following dimensionless form we express lengths in units of the scale  $l_0 = \sqrt{\hbar/m\omega_z}$ , time in units of  $t_0 = \omega_z^{-1}$ , angular frequency in units of

$\omega_z$ , energy in units of  $\hbar\omega_z$  and density  $|\psi|^2$  in units of  $l^{-3}$

$$i \frac{\partial \psi(\mathbf{r}, t)}{\partial t} = \left[ -\frac{1}{2} \nabla^2 + \frac{1}{2} [\omega_\rho^2(x^2 + y^2) + z^2] + 4\pi a N |\psi(\mathbf{r}, t)|^2 + 3a_{\text{dd}} N \int U_{\text{dd}}(\mathbf{R}) |\psi(\mathbf{r}', t)|^2 d\mathbf{r}' + \gamma_{\text{LHY}} N^{3/2} |\psi(\mathbf{r}, t)|^3 - \Omega l_z \right] \psi(\mathbf{r}, t). \quad (6)$$

Here and in the following, without any risk of confusion, we are representing both the dimensional and the dimensionless variables by the same symbols. Equation (6) can be obtained from the variational principle

$$i \frac{\delta \psi}{\delta t} = \frac{\delta E}{\delta \psi^*}, \quad (7)$$

from which we obtain the following expression for the energy functional representing the energy per atom in a stationary giant vortex in the rotating dipolar BEC

$$E = \int d\mathbf{r} \left[ \frac{1}{2} |\nabla \psi(\mathbf{r})|^2 + \frac{1}{2} \{ \omega_\rho^2(x^2 + y^2) + z^2 \} |\psi(\mathbf{r})|^2 + \frac{3}{2} a_{\text{dd}} N |\psi(\mathbf{r})|^2 \int U_{\text{dd}}(\mathbf{R}) |\psi(\mathbf{r}')|^2 d\mathbf{r}' + 2\pi N a |\psi(\mathbf{r})|^4 + \frac{2\gamma_{\text{LHY}}}{5} N^{3/2} |\psi(\mathbf{r})|^5 - i\Omega \psi^*(\mathbf{r}) \left( y \frac{\partial}{\partial x} - x \frac{\partial}{\partial y} \right) \psi(\mathbf{r}) \right]. \quad (8)$$

### 3. Numerical Results

The partial differential GP equation (6) is solved numerically employing the split-time-step Crank-Nicolson method [65], using the available C and FORTRAN programs [62]. and their open-multiprocessing [66, 67] versions. The imaginary-time propagation was used to find the stationary giant vortex state and the real-time propagation to test its dynamical stability. The space steps employed for the solution of Eq. (6) are  $dx = dy = 0.1$  and  $dz = 0.125$ , and the corresponding time steps in imaginary- and real-time propagations are  $dt = 0.1 \times (dxdydz)^{2/3}$  and  $dt = 0.0125 \times (dxdydz)^{2/3}$ , respectively.

For the appearance of a giant vortex, we need a strongly dipolar atom with  $a_{\text{dd}} > a$ . For  $a_{\text{dd}} < a$ , the system becomes repulsive and behaves more like a nondipolar BEC and no giant vortex can be formed. Although,  $a_{\text{dd}} = 130.8a_0$  for  $^{164}\text{Dy}$  atoms, we have a certain flexibility in fixing the scattering length  $a$ , as the scattering length can be modified employing the Feshbach resonance technique [68] by manipulating an external electromagnetic field. In this study we take the

scattering length in the domain  $86a_0 > a > 80a_0$ , close to the previously used values  $a = 92(8)a_0$  [50, 55, 69] and  $a = 88a_0$  [51]. For smaller values of  $a$  ( $\lesssim 80a_0$ ) these states are unstable and collapses, whereas for larger  $a$  ( $\gtrsim 87a_0$ ) these states decay to multiple states of unit angular momentum. With the reduction of contact repulsion, using a Feshbach resonance [68], the choice of scattering length in the region  $86a_0 > a > 80a_0$  has the advantage of slightly increasing the net attraction, which is found to facilitate the formation of a giant vortex upon rotation. The number of atoms will be taken as  $N = 200000$ , which favors the formation of giant vortices. For  $N \lesssim 140000$  these states become unstable and can not be found in imaginary-time propagation. For dysprosium atoms  $m(^{164}\text{Dy}) \approx 164 \times 1.66054 \times 10^{-27}$  kg. Consequently, for  $\omega_z = 2\pi \times 167$  Hz, used in this study as in some recent experiments with  $^{164}\text{Dy}$  atoms [57, 58], the unit of length is  $l_0 = \sqrt{\hbar/m\omega_z} = 0.6075$   $\mu\text{m}$  and the unit of time  $t_0 = 0.9530$  ms. It is true that the angular frequency  $\omega_z$  is the same in both cases, but the quasi-2D (two dimensional) trap shape in Refs. [57, 58] is very different from the trap in the present case ( $\omega_\rho = 0.75\omega_z$ ), with a much larger trap frequency in the transverse direction, resulting in a different configuration. If the angular frequency of the transverse trap is very different from this value ( $0.75\omega_z$ ) the giant vortices may not be stabilized. The demonstration of a giant vortex is best confirmed by a hollow region in the integrated 2D density  $n_{2D}(x, y)$  defined by

$$n_{2D}(x, y) = \int_{-\infty}^{\infty} dz |\psi(x, y, z)|^2. \quad (9)$$

To facilitate the numerical simulation of a giant vortex by imaginary-time propagation we use the following phase-imprinted Gaussian initial state, as in Ref. [70],

$$\psi(\mathbf{r}) = (x + iy)^l \times \exp\left[-\frac{x^2 + y^2}{2\delta_\rho^2} - \frac{z^2}{2\delta_z^2}\right], \quad (10)$$

where  $\delta_\rho$  and  $\delta_z$  are width parameters of the Gaussian state and  $l$  its angular momentum. To find a giant vortex with a fixed angular momentum the angular frequency of rotation is gradually increased in imaginary-time propagation till the giant vortex state can be obtained. The angular momentum of the obtained giant vortex is confirmed from a contour plot of the phase of the wave function  $\psi(x, y, 0)$  in the  $x - y$  plane. The phase jump of  $2\pi l$  around a closed contour containing the  $x = y = 0$  point confirms a giant vortex of angular momentum  $l$ , viz. Eq. (1).

Using the initial function (10) in imaginary-time propagation we obtain the normal states for angular momentum  $l = 0, 1$  as well as the giant-vortices of different

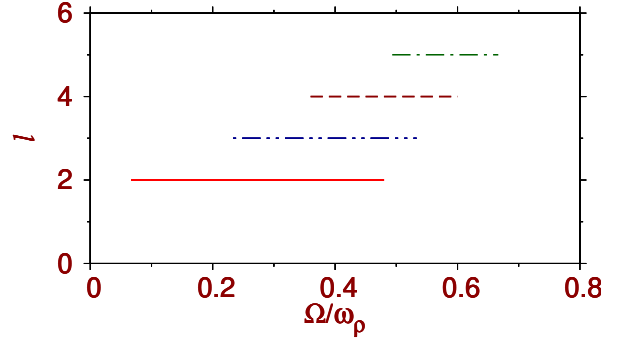


Figure 1: The range of angular frequency of rotation  $\Omega/\omega_\rho$  for the appearance of a giant vortex of angular momentum  $l$  ( $5 \geq l \geq 2$ ). The parameters of the model are  $N = 200000$ ,  $a = 80a_0$ ,  $a_{\text{dd}} = 130.8a_0$ ,  $\omega_z = 2\pi \times 167$  Hz,  $\omega_\rho = 0.75\omega_z$ . The plotted results in all figures are dimensionless.

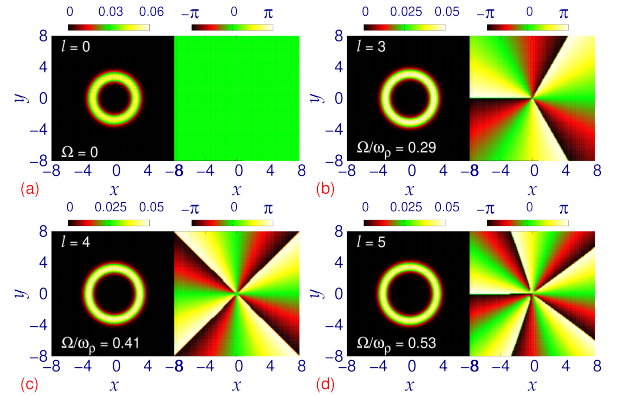


Figure 2: Contour plot of dimensionless 2D density  $n_{2D}(x, y)$  (left panel) and phase of the wave function  $\psi(x, y, 0)$  (right panel) of the giant-vortices of angular momentum and angular velocity of rotation (a)  $l = 0, \Omega = 0$ , (b)  $l = 3, \Omega/\omega_\rho = 0.29$ , (c)  $l = 4, \Omega/\omega_\rho = 0.41$ , (d)  $l = 5, \Omega/\omega_\rho = 0.53$ . The parameters of the model are  $N = 200000$ ,  $a = 80a_0$ ,  $a_{\text{dd}} = 130.8a_0$ ,  $\omega_z = 2\pi \times 167$  Hz,  $\omega_\rho = 0.75\omega_z$ .

angular momentum  $l = 2$  to  $5$ . As  $l$  is increased, the angular velocity of rotation  $\Omega$  is also gradually increased until a converged result is obtained for the giant vortex. Although, the state for  $l \leq 5$  is a stationary state with ring topology (a cylindrical state with a coaxial hole) obtainable in a imaginary-time propagation calculation, for larger  $l$  this is not so. For larger  $l$ , the axially-symmetric hollow cylindrical state breaks into multiple fragments due to large centrifugal force. A giant vortex with fixed angular momentum  $l$  can be obtained for the rotational frequency  $\Omega$  between two limiting values  $\Omega_2 > \Omega > \Omega_1$ . This is illustrated in Fig. 1 through a plot of range of angular frequency of rotation for dif-

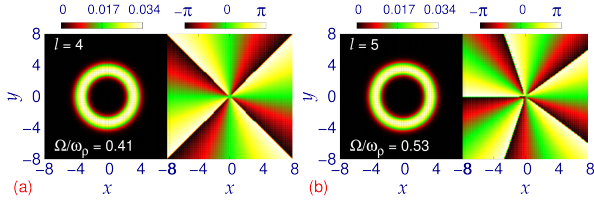


Figure 3: Contour plot of dimensionless 2D density  $n_{2D}(x, y)$  (left panel) and phase of the wave function  $\psi(x, y, 0)$  (right panel) of the giant vortices of angular momentum and angular velocity of rotation (a)  $l = 4$ ,  $\Omega/\omega_p = 0.41$ , (b)  $l = 5$ ,  $\Omega/\omega_p = 0.53$ . The parameters of the model are  $N = 200000$ ,  $a = 85a_0$ ,  $a_{dd} = 130.8a_0$ ,  $\omega_z = 2\pi \times 167$  Hz,  $\omega_p = 0.75\omega_z$ .

ferent angular momentum  $l$  of a giant vortex. Each line in this plot shows the extension of  $\Omega$  values for which a giant vortex of a specific angular momentum  $l$  can be obtained. The window of  $\Omega$  values  $\Delta \equiv \Omega_2 - \Omega_1$  for stabilizing a giant vortex of angular momentum  $l$  reduces as  $l$  increases. The smaller threshold  $\Omega_1$  of the rotational frequency for the formation of a giant vortex increases with the angular momentum  $l$ . The  $l = 1$  vortex is easily obtained for  $\Omega = 0.10$  (not shown here).

The giant vortex states for different  $l$  are illustrated through a contour plot of dimensionless 2D density  $n_{2D}(x, y)$  (left panel) and its phase (right panel) in Fig. 2. All these states including the nonrotating  $l = 0$  state have a ring topology. Similar ring-shaped density was obtained in a harmonically-trapped nonrotating dipolar BEC in Ref. [54] for scattering length  $a = 100a_0$  ( $a/a_{dd} = 0.77$ ), as well as in Refs. [53, 59] for similar sets of parameters. We illustrate the results, contour plot of quasi-2D density  $n_{2D}(x, y)$  (left panel) and phase (right panel) of the giant vortices in Fig. 2 for (a)  $l = 0$ ,  $\Omega = 0$ , (b)  $l = 3$ ,  $\Omega/\omega_p = 0.29$ , (c)  $l = 4$ ,  $\Omega/\omega_p = 0.41$ , (d)  $l = 5$ ,  $\Omega/\omega_p = 0.53$ . The central hollow region of the giant vortex is very prominent in this figure. We find that the radius of the central hollow region increases monotonically as the angular momentum of the giant vortex increases. In these plots, the phase drop of the wave function  $\psi(x, y, 0)$  along a closed path including the origin is  $2\pi l$  for a giant vortex of angular momentum  $l$ .

In Fig. 2 the inner hollow region of the giant vortex obtained with  $N = 200000$ ,  $a = 80a_0$ ,  $\omega_z = 2\pi \times 167$  Hz,  $\omega_p = 0.75\omega_z$  is quite sharp and pronounced and its radius increases monotonically with angular momentum  $l$ . It is of utmost interest to investigate how the formation of the giant vortex changes as the parameters of the model are modified. As the scattering length  $a$  is increased, the contact repulsion increases, but the inner

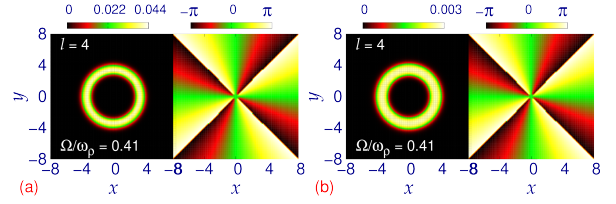


Figure 4: Contour plot of dimensionless 2D density  $n_{2D}(x, y)$  (left panel) and phase of the wave function  $\psi(x, y, 0)$  (right panel) of the giant vortices of angular momentum  $l = 4$  for (a)  $N = 250000$ ,  $\omega_z = 2\pi \times 167$  Hz (b)  $N = 200000$ ,  $\omega_z = 2\pi \times 200$  Hz. Other parameters of the model are the same as in Fig. 2.

radius of the giant vortex remains practically the same as can be found from the contour plot of the  $l = 4, 5$  giant vortices in Fig. 3 for  $N = 200000$ ,  $a = 85a_0$ ,  $\omega_z = 2\pi \times 167$  Hz, by comparing with the contour plot in Fig. 2 for  $a = 80a_0$ , with other parameters unchanged. Incidentally, the value  $a = 88a_0$  is a reliable estimate of the scattering length used in many studies [51, 52]. With further increase of  $a$ , for  $a \gtrsim 85a_0$ , the giant vortices with large  $l$  gradually cease to exist. For example, for  $a = 87a_0$ , only the giant vortices with  $l \leq 4$  are found to exist. For even larger  $a$ , for example, for  $a = 92a_0$ , the contact repulsion increases and, consequently, the giant vortex state loses the shell-shaped structure and a Gaussian-type BEC in the shape of a normal solid cylinder with only  $l = 1$  vortices are obtained in imaginary-time propagation (not explicitly shown here).

We next investigate the fate of the giant vortices as other parameters of the model are changed. If  $N$  is decreased below a critical value, the cylindrical-shell-shaped states are not possible and only fragmented droplet-type states appear. For  $\omega_z = 2\pi \times 167$  Hz this happens for  $N \approx 100000$  (not explicitly shown here). However, the axially-symmetric giant vortices survive for larger  $N$  as illustrated in Fig. 4(a) for  $N = 250000$  with all other parameters unchanged. Finally, we study the fate of the giant vortices as the axial frequency  $\omega_z$  is changed. As  $\omega_z$  is reduced further, these states disappear, for example for  $\omega_z = 2\pi \times 100$  Hz, when multi-fragment states appear (not shown here). However, these states survive for larger values of  $\omega_z$  as illustrated in Fig. 4(b) for  $\omega_z = 2\pi \times 200$  Hz with other parameters unchanged. However, if the transverse trapping frequency  $\omega_p$  is reduced below  $\omega_p = 0.60\omega_z$ , or increased above  $\omega_p = 0.90\omega_z$ , these states disappear. In the former case, the system is no longer strongly dipolar and in the latter case the stronger trapping frequency transforms the hollow cylindrical states to the shape of a solid cylinder.

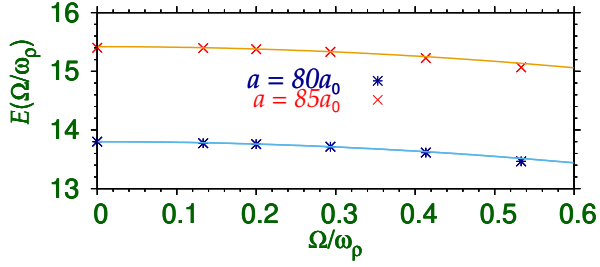


Figure 5: The energy per atom of the giant vortex of different angular momentum as a function of the angular velocity of rotation for  $a = 80a_0$  and  $a = 85a_0$ . The points correspond to different angular-momentum states ( $l = 0$  to  $5$ ) as obtained from Eq. (8); the increase in angular momentum of the giant vortex correspond to a decrease in energy. The lines are the theoretical estimate (11) with  $I = 2$ .

Fetter made the following theoretical estimate of the energy per atom of a nondipolar dilute rotating BEC in a harmonic trap [6]

$$E(\Omega/\omega_p) = E(0) - \frac{I}{2} \left( \frac{\Omega}{\omega_p} \right)^2 \quad (11)$$

where  $I$  is the moment of inertia of rigid-body rotation of an atom of the superfluid and  $\frac{1}{2}I(\Omega/\omega_p)^2$  is the rotational kinetic energy. We have applied this estimate to the present case of giant vortex in a strongly dipolar BEC of  $^{164}\text{Dy}$  atoms including the LHY interaction. A plot of energy  $E(\Omega/\omega_p)$  of Eq. (8) versus the angular velocity of rotation  $\Omega/\omega_p$  for the giant vortices of different angular momentum,  $l = 0$  to  $5$ , is displayed in Fig. 5, for  $a = 80a_0$  and  $85a_0$ , which confirms the universal behavior of the rotational energy given by Eq. (11), where for  $E(0)$  we have taken the numerically obtained energy (8) for  $\Omega = 0$ . The points correspond to the different vortices ( $l \leq 5$ ) illustrated in Fig. 2; the energy decreases with increasing angular momentum  $l$  in a monotonic fashion. The full lines are the theoretical estimates (11) for  $I = 2$ . The moment of inertia  $I$  was obtained from Eq. (11) using the numerical energy for  $\Omega = 0$  and another energy for  $\Omega \neq 0$ . It is pleasing to see that the Fetter's universal estimate of energy for a dilute BEC works very well for a strongly dipolar dense BEC for two values of the scattering lengths using the same moment of inertia  $I = 2$ .

To demonstrate the dynamical stability of the giant vortices, we consider the giant vortex of Fig 2(d) with  $l = 3$ ,  $a = 80a_0$  and  $\Omega/\omega_p = 0.29$  and change  $\Omega/\omega_p$  to  $0.285$  in the model equation (6) maintaining other parameters unchanged. Using the converged imaginary-time wave function as the initial state, we perform real-time propagation of Eq. (6) with  $\Omega/\omega_p = 0.285$  for 100

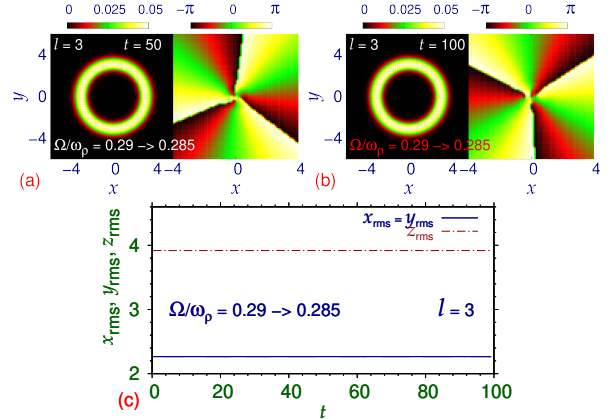


Figure 6: The same as in Fig. 2 of the giant vortex of Fig. 2(d) of angular momentum  $l = 3$  at times (a)  $t = 50$  (b)  $t = 100$  during real-time propagation using the imaginary-time wave function as the initial state after changing the rotational velocity  $\Omega/\omega_p$  from  $0.29$  to  $0.285$ . The evolution of the rms sizes  $x_{\text{rms}}$ ,  $y_{\text{rms}}$ , and  $z_{\text{rms}}$  versus time for the dynamics of (c) Figs. 6(a)-(b). Other parameters of the model are the same as in Fig. 2.

units of time (about 100 ms in the present case). The density and the phase of the real-time wave function at times  $t = 50$  and  $100$  are exhibited in Figs. 6(a) and (b). The phase drop around a closed circular path at the center in (a)-(b) is  $6\pi$ , corresponding to an angular momentum of  $l = 3$ . The evolution of the root-mean-square (rms) sizes during the real-time propagation exhibited in Figs. 6(a)-(b) is shown in Figs. 6(c). The circularly-symmetric density distribution and the correct phase drop at the center in Figs. 6(a) and (b) at  $t = 50$  and  $t = 100$  as well as the steady oscillation of the rms sizes with a very small amplitude in Figs. 6(c) guarantee the dynamical stability of the giant vortices. As we do not know the different loss rates of the dipolar BEC, we did not include any dissipation in this study. A demonstration of the dynamical stability including appropriate dissipations is beyond the scope of the present investigation, and would be the subject of a future investigation.

It has been demonstrated that ring-shaped densities with nondipolar [71] and dipolar [72] condensates can support multiply charged circulation even at zero rotation frequency, called persistent currents, that differ from vortices as their existence do not require rotation, contrary to vortices. Typically, a persistent current was generated by imprinting a vortex on a stable ring-shaped condensate [71] in an appropriate (non-harmonic) trap. We verified that such persistent current is not possible in the present condensate in the absence of rotation. To

demonstrate we considered the non-rotating condensate of Fig. 2(a) in a harmonic trap and imprinted its wave function with a multiply-charged vortex and performed real-time simulation with this initial state for  $\Omega = 0$ . The multiply-charged vortex is immediately destroyed demonstrating the absence of persistent current in the present case. Also, we have seen that in imaginary-time propagation the giant vortices do not exist for  $\Omega = 0$ , viz. Fig. 1, corroborating the fact that the present  $l > 1$  states are giant vortices.

#### 4. Summary

In conclusion, we have demonstrated the possibility of generating a dynamically stable giant vortex of angular momentum  $l = 2$  to 5 in a harmonically-trapped strongly-dipolar BEC of  $^{164}\text{Dy}$  atoms, for parameters similar to those used in recent studies [50, 57, 58] on this system, by employing imaginary- and real-time propagation of an improved mean-field equation including a LHY interaction [44] appropriately modified [45] for dipolar atoms. The giant vortices appear for number of atoms  $N$  in the range  $140000 \lesssim N \lesssim 250000$ , angular trap frequency in the range  $2\pi \times 130 \text{ Hz} \lesssim \omega_z \lesssim 2\pi \times 230 \text{ Hz}$  and  $0.60 \lesssim \omega_\rho/\omega_z \lesssim 0.90$  and for scattering length in the range  $80a_0 \lesssim a \lesssim 85a_0$ , viz. Figs. 3 and 4. A large dipole moment is essential for the formation of a strongly-dipolar BEC necessary for generating a giant vortex. The energy of the giant vortices (8) are in agreement with the theoretical estimate (11) [6], viz. Fig. 5. The dynamical stability of the giant vortices was established by real-time propagation upon a small perturbation of the trap frequency, employing the converged imaginary-time wave function as the initial state. The present study may initiate new avenues of theoretical and experimental research in the area of cold atoms.

#### CRedit authorship contribution statement

L. E. Young-S. and S. K. Adhikari: Conceptualization, Methodology, Validation, Investigation, Writing – original draft, Writing – review and editing, Visualization.

#### Declaration of competing interest

The authors declare that they have no known competing financial interests or personal relationships that could have appeared to influence the work reported in this paper.

#### Data availability

No data was used for the research described in the article.

#### Acknowledgments

LEY-S. acknowledges partial financial support by the Vicerrectoría de Investigaciones - Universidad de Cartagena, Colombia through Projects 004-2023 and 064-2023. SKA acknowledges partial support by the CNPq (Brazil) grant 301324/2019-0. The use of the supercomputing cluster of the Universidad de Cartagena is acknowledged.

#### References

- [1] M. H. Anderson, J. R. Ensher, M. R. Matthews, C. E. Wieman, E. A. Cornell, *Science* 269, 198 (1995).
- [2] K. B. Davis, M. -O. Mewes, M. R. Andrews, N. J. van Druten, D. S. Durfee, D. M. Kurn, W. Ketterle, *Phys. Rev. Lett.* 75, 3969 (1995).
- [3] L. Onsager, *Nuovo Cimento.* 6, 249 supp 2 (1949).
- [4] R. P. Feynman, *Prog. Low Temp. Phys.* 1, 17 (1955).
- [5] A. A. Abrikosov, *Zh. Eksp. Teor. Fiz.* 32, 1442 (1957); [English Transla. A. A. Abrikosov, *Sov. Phys.—JETP* 5, 1174 (1957).]
- [6] A. L. Fetter, *Rev. Mod. Phys.* 81, 647 (2009).
- [7] K. W. Madison, F. Chevy, W. Wohlleben, J. Dalibard, *Phys. Rev. Lett.* 84, 806 (2000).
- [8] P. W. Courteille, V. S. Bagnato, V. I. Yukalov, *Laser Phys.* 11, 659 (2001).
- [9] V. I. Yukalov, *Laser Phys. Lett.* 1, 435 (2014).
- [10] J. R. Abo-Shaeer, C. Raman, W. Ketterle, *Phys. Rev. Lett.* 88, 070409 (2002).
- [11] M. R. Matthews, B. P. Anderson, P. C. Haljan, D. S. Hall, M. J. Holland, J. E. Williams, C. E. Wieman, E. A. Cornell, *Phys. Rev. Lett.* 83, 3358 (1999).
- [12] J. R. Abo-Shaeer, C. Raman, J. M. Vogels, W. Ketterle, *Science* 292, 476 (2001).
- [13] P. C. Haljan, B. P. Anderson, I. Coddington, E. A. Cornell, *Phys. Rev. Lett.* 86, 2922 (2001).
- [14] V. Schweikhard, I. Coddington, P. Engels, S. Tung, E. A. Cornell, *Phys. Rev. Lett.* 93, 210403 (2004).
- [15] N. Ghazanfari, A. Keles, M. Ö Oktel, *Phys. Rev. A* 89, 025601 (2014).
- [16] R. K. Kumar, L. Tomio, B. A. Malomed, A. Gammal, *Phys. Rev. A* 96, 063624 (2017).
- [17] R. K. Kumar, L. Tomio, A. Gammal, *Phys. Rev. A* 99, 043606 (2019).
- [18] K. Kasamatsu, K. Sakashita, *Phys. Rev. A* 97, 053622 (2018).
- [19] A. E. Leanhardt, Y. Shin, D. Kielpinski, D. E. Pritchard, W. Ketterle, *Phys. Rev. Lett.* 90, 140403 (2003).
- [20] S.-W. Su, C.-H. Hsueh, I.-K. Liu, T.-L. Horng, Y.-C. Tsai, S.-C. Gou, W. M. Liu, *Phys. Rev. A* 84, 023601 (2011).
- [21] M. Cipriani, M. Nitta, *Phys. Rev. Lett.* 111, 170401 (2013)
- [22] P. Mason, A. Aftalion, *Phys. Rev. A* 84, 033611 (2011).
- [23] P. Švančara, P. Smaniotta, L. Solidoro, J. F. MacDonald, S. Patrick, R. Gregory, C. F. Barenghi, S. Weinfurter, *Nature* 628, 66 (2024).
- [24] S. L. Braunstein, P. van Loock, *Rev. Mod. Phys.* 77, 513 (2005).

- [25] C. Weedbrook, S. Pirandola, R. García-Patrón, N. J. Cerf, T. C. Ralph, J. H. Shapiro, S. Lloyd, *Rev. Mod. Phys.* 84, 621 (2012).
- [26] E. Lundh, *Phys. Rev. A* 65, 043604 (2002).
- [27] K. Kasamatsu, M. Tsubota, M. Ueda, *Phys. Rev. A* 66, 053606 (2002).
- [28] U. R. Fischer and G. Baym, *Phys. Rev. Lett.* 90, 140402 (2003).
- [29] A. Aftalion, I. Danaila, *Phys. Rev. A* 69, 033608 (2004).
- [30] A. L. Fetter, *Phys. Rev. A* 64, 063608 (2001).
- [31] J. Kim, A. Fetter, *Phys. Rev. A* 72, 023619 (2005).
- [32] T. P. Simula, S. M. M. Virtanen, M. M. Salomaa, *Phys. Rev. A* 65, 033614 (2002).
- [33] A. C. White, *Phys. Rev. A* 109, 013301 (2024).
- [34] S. K. Adhikari, *Laser Phys. Lett.* 16, 085501 (2019).
- [35] P. Engels, I. Coddington, P. C. Haljan, V. Schweikhard, E. A. Cornell, *Phys. Rev. Lett.* 90, 170405 (2003).
- [36] T. P. Simula, A. A. Penckwitt, R. J. Ballagh, *Phys. Rev. Lett.* 92, 060401 (2004).
- [37] G. Gauthier, M. T. Reeves, X. Yu, A. S. Bradley, M. A. Baker, T. A. Bell, H. Rubinsztein-Dunlop, M. J. Davis, T. W. Neely, *Science* 364, 1264 (2019).
- [38] J. Qin, G. Dong, B. A. Malomed, *Phys. Rev. A* 94, 053611 (2016).
- [39] S.-J. Yang, Q.-S. Wu, S.-N. Zhang, S. Feng, *Phys. Rev. A* 77, 033621 (2008).
- [40] X.-Q. Xu, J. H. Han, *Phys. Rev. Lett.* 107, 200401 (2011).
- [41] Y. Zhao, J. An, C.-De Gong, *Phys. Rev. A* 87, 013605 (2013).
- [42] S. B. Prasad, T. Bland, B. C. Mulkerin, N. G. Parker, A. M. Martin, *Phys. Rev. A* 100, 023625 (2019).
- [43] R. M. W. Van Bijnen, A. J. Dow, D. H. J. O'Dell, N. G. Parker, A. M. Martin, *Physical Review A* 80, 033617 (2009).
- [44] T. D. Lee, K. Huang, C. N. Yang, *Phys. Rev.* 106, 1135 (1957).
- [45] A. R. P. Lima, A. Pelster, *Phys. Rev. A* 84, 041604(R) (2011).
- [46] A. R. P. Lima, A. Pelster, *Phys. Rev. A* 86, 063609 (2012).
- [47] R. Schützhold, M. Uhlmann, Y. Xu, U. R. Fischer, *Int. J. Mod. Phys. B* 20, 3555 (2006).
- [48] H. Kadau, M. Schmitt, M. Wenzel, C. Wink, T. Maier, I. Ferrier-Barbut, T. Pfau, *Nature* 530, 194 (2016).
- [49] M. Schmitt, M. Wenzel, F. Böttcher, I. Ferrier-Barbut, T. Pfau, *Nature* 539, 259 (2016).
- [50] L. Chomaz, I. Ferrier-Barbut, F. Ferlaino, B. Laburthe-Tolra, B. L. Lev, T. Pfau, *Rep. Prog. Phys.* 86, 026401 (2023).
- [51] E. Poli, T. Bland, C. Politi, L. Klaus, M. A. Norcia, F. Ferlaino, R. N. Bisset, and L. Santos, *Phys. Rev. A* 104, 063307 (2021).
- [52] L. E. Young-S. and S. K. Adhikari, *Phys. Rev. A* 105, 033311 (2022).
- [53] J. Hertkorn, J.-N. Schmidt, M. Guo, F. Böttcher, K. S. H. Ng, S. D. Graham, P. Uerlings, T. Langen, M. Zwierlein, and T. Pfau, *Phys. Rev. Res.* 3, 033125 (2021).
- [54] Y.-C. Zhang, T. Pohl, and F. Maucher, *Phys. Rev. A* 104, 013310 (2021).
- [55] Y. Tang, A. Sykes, N. Q. Burdick, J. L. Bohn, B. L. Lev, *Phys. Rev. A* 92, 022703 (2015).
- [56] L. Chomaz, D. Petter, P. Ilzhöfer, G. Natale, A. Trautmann, C. Politi, G. Durastante, R. M. W. van Bijnen, A. Patscheider, M. Sohmen, M. J. Mark, F. Ferlaino, *Phys. Rev. X* 9, 021012 (2019).
- [57] M. A. Norcia, C. Politi, L. Klaus, E. Poli, M. Sohmen, M. J. Mark, R. Bisset, L. Santos, F. Ferlaino, *Nature* 596, 357 (2021).
- [58] T. Bland, E. Poli, C. Politi, L. Klaus, M. A. Norcia, F. Ferlaino, L. Santos, R. N. Bisset, *Phys. Rev. Lett.* 128, 195302 (2022).
- [59] L. E. Young-S., S. K. Adhikari, *Phys. Rev. A* 108, 053323 (2023).
- [60] T. Lahaye, C. Menotti, L. Santos, M. Lewenstein, T. Pfau, *Rep. Prog. Phys.* 72, 126401 (2009).
- [61] R. N. Bisset, R. M. Wilson, D. Baillie, P. B. Blakie, *Phys. Rev. A* 94, 033619 (2016).
- [62] R. Kishor Kumar, L. E. Young-S., D. Vudragović, A. Balaž, P. Muruganandam, S. K. Adhikari, *Comput. Phys. Commun.* 195, 117 (2015).
- [63] V. I. Yukalov, *Laser Phys.* 28, 053001 (2018).
- [64] L. D. Landau, E. M. Lifshitz, *Mechanics*, Pergamon Press, Oxford (1960), Section 39.
- [65] P. Muruganandam, S. K. Adhikari, *Comput. Phys. Commun.* 180, 1888 (2009).
- [66] L. E. Young-S., P. Muruganandam, A. Balaž, S. K. Adhikari, *Comput. Phys. Commun.* 286, 108669 (2023).
- [67] V. Lončar, L. E. Young-S., S. Škrbić, P. Muruganandam, S. K. Adhikari, A. Balaž, *Comput. Phys. Commun.* 209, 190 (2016).
- [68] C. Chin, R. Grimm, P. Julienne, E. Tiesinga, *Rev. Mod. Phys.* 82, 1225 (2010).
- [69] T. Maier, I. Ferrier-Barbut, H. Kadau, M. Schmitt, M. Wenzel, C. Wink, T. Pfau, K. Jachymski, P. S. Julienne, *Phys. Rev. A* 92, 060702(R) (2015).
- [70] A. E. Leanhardt, A. Görlitz, A. P. Chikkatur, D. Kielpinski, Y. Shin, D. E. Pritchard, W. Ketterle, *Phys. Rev. Lett.* 89, 190403 (2002).
- [71] C. Ryu, M. F. Andersen, P. Cladé, Vasant Natarajan, K. Helmerston, W. D. Phillips, *Phys. Rev. Lett.* 99, 260401 (2007).
- [72] F. Malet, G. M. Kavoulakis, S. M. Reimann, *Phys. Rev. A* 84, 043626 (2011).